PCCP

PAPER

View Article Online
View Journal | View Issue

Cite this: *Phys. Chem. Chem. Phys.*, 2024, **26**, 10769

Exploring the large chemical space in search of thermodynamically stable and mechanically robust MXenes *via* machine learning†

Jaejung Park,[a] Minseon Kim,[b] Heekyu Kim,[a] Jaejun Lee,[a] Inhyo Lee,[b] Haesun Park,[c] Anna Lee,[a] Kyoungmin Min *[b] and Seungchul Lee*[d]

To effectively utilize MXenes, a family of two-dimensional materials, in various applications that include thermoelectric devices, semiconductors, and transistors, their thermodynamic and mechanical properties, which are closely related to their stability, must be understood. However, exploring the large chemical space of MXenes and verifying their stability using first-principles calculations are computationally expensive and inefficient. Therefore, this study proposes a machine learning (ML)-based high-throughput MXene screening framework to identify thermodynamically stable MXenes and determine their mechanical properties. A dataset of 23 857 MXenes with various compositions was used to validate this framework, and 48 MXenes were predicted to be stable by ML models in terms of heat of formation and energy above the convex hull. Among them, 45 MXenes were validated using density functional theory calculations, of which 23 MXenes, including Ti_2CClBr and Zr_2NCl_2, have not been previously known for their stability, confirming the effectiveness of this framework. The in-plane stiffness, shear moduli, and Poisson's ratio of the 45 MXenes were observed to vary widely according to their constituent elements, ranging from 90.11 to 198.02 N m^{-1}, 64.00 to 163.40 N m^{-1}, and 0.19 to 0.58, respectively. MXenes with Group-4 transition metals and halogen surface terminations were shown to be both thermodynamically stable and mechanically robust, highlighting the importance of electronegativity difference between constituent elements. Structurally, a smaller volume per atom and minimum bond length were determined to be preferable for obtaining mechanically robust MXenes. The proposed framework, along with an analysis of these two properties of MXenes, demonstrates immense potential for expediting the discovery of stable and robust MXenes.

Received 30th December 2023,
Accepted 14th March 2024

DOI: 10.1039/d3cp06337b

rsc.li/pccp

1. Introduction

MXenes[1] are a class of two-dimensional (2D) materials that have attracted considerable attention because of their outstanding physicochemical and electronic properties, and have numerous potential applications as electrodes in rechargeable batteries,[2,3] catalysts in the hydrogen evolution reaction,[4] and thermoelectric devices.[5,6] These materials are composed of transition metal carbides, nitrides, and carbonitrides with the general chemical formula of $M_{n+1}X_nT_x$, where M represents the transition metal, X represents carbon and/or nitrogen, T represents the surface termination, and n is typically 1, 2, or 3. An advantage of MXenes that sets them apart from other conventional 2D materials such as graphene is their large chemical space,[7] which allows the tuning of their properties through the selection of different transition metals, surface terminations, and layer thicknesses. Because the bonds between M and X and those between M and T influence the different properties of MXenes, such as their thermodynamic and mechanical properties,[8,9] MXenes can be customized by altering such bonds to meet the specific requirements of various applications. Moreover, this large chemical space can be further expanded by considering non-stoichiometric MXenes, which do not follow a general chemical formula. For example, MXenes with two different surface terminations $\left(M_{n+1}X_nT'_{x-y}T''_y\right)$, two types of transition metals $\left(M'_{n-m+1}M''_mX_nT_x\right)$, and distinct surface terminations and transition metals $\left(M'_{n-m+1}M''_mX_nT'_{x-y}T''_y\right)$ exist. They have been comprehensively studied as a new family in the field of

[a] *Department of Mechanical Engineering, Pohang University of Science and Technology (POSTECH), Pohang, Republic of Korea*
[b] *School of Mechanical Engineering, Soongsil University, Seoul, Republic of Korea. E-mail: kmin.min@ssu.ac.kr*
[c] *School of Integrative Engineering, Chung-Ang University, Seoul, Republic of Korea*
[d] *Department of Mechanical Engineering, Korea Advanced Institute of Science and Technology (KAIST), Daejeon, Republic of Korea. E-mail: seunglee@kaist.ac.kr*

† Electronic supplementary information (ESI) available. See DOI: https://doi.org/10.1039/d3cp06337b

MXenes;[10–12] consequently, MXenes have become the most extensive family of 2D materials.

As an efficient tool to explore the large family of MXenes, a high-throughput computational screening (HTCS) method based on first-principles calculations, such as density functional theory (DFT)[13–16] and molecular dynamic,[17,18] is widely employed. This method leverages the accuracy of first-principles calculations in predicting the electronic structure, adsorption properties, thermoelectric properties, and other relevant properties of MXenes to narrow down the number of candidates and, consequently, identify a MXene that is the most suitable for a particular application. For instance, Zeng *et al.*[14] applied the HTCS to 64 candidate MXenes to sequentially calculate their thermodynamic properties, specifically the heat of formation and hydrogen adsorption properties, using DFT. They identified MXenes as suitable catalysts for the hydrogen evolution reaction. Similarly, Guha *et al.*[19] investigated MXene transistors with low-resistive contacts and sequentially calculated electronic (such as the bandgap and in-plane static dielectric constant), structural, and thermodynamic properties using DFT. Other studies employing HTCS have successfully identified optimal MXenes by computing various properties, including mechanical properties such as in-plane stiffness,[20] thermoelectric properties such as Seebeck coefficients,[21] and magnetic properties such as ferroelectricity.[22] The ability to accurately identify and screen various properties of MXenes using computational methods is crucial in HTCS, which has made HTCS an invaluable method in MXene research.

Among the various properties of MXenes that are commonly considered in HTCS studies, thermodynamic properties such as heat of formation (ΔH) and energy above the convex hull (ΔH_{hull}), as well as mechanical properties such as in-plane stiffness and shear modulus, are significantly important.[9] First, the thermodynamic properties serve as critical indicators for predicting the thermodynamic stability of MXenes. MXenes with $\Delta H < 0$ eV per atom and 0 eV per atom $\leq \Delta H_{\text{hull}} \leq$ 0.1 eV per atom can be considered to be thermodynamically stable and these criteria have been widely used in previous studies.[23,24] Thermodynamically stable MXenes have a low probability of decomposing or reacting with other substances, making them desirable for practical applications. Moreover, their higher likelihood of remaining stable during the synthesis process enhances the feasibility of production. Second, the mechanical properties are essential characteristics that must be evaluated to utilize MXenes in practical applications, such as energy storage and transistors. For examples, MXenes have been extensively studied as electrode materials for secondary batteries such as lithium- and aluminum-ion batteries.[2,3,13] In these applications, the mechanical properties of MXenes play a crucial role in maintaining the structural stability of the electrodes, enabling them to withstand the deformation caused by volume expansion and contraction during the charging and discharging processes.[8,9,25] Therefore, calculating the thermodynamic and mechanical properties of candidate MXenes using DFT in the HTCS can not only gradually narrow down the number of candidate MXenes but also ensure that the MXenes with the best performance for specific applications are both thermodynamically stable and mechanically robust.

Despite the remarkable practicality of HTCS, exploring the vast chemical spaces of MXenes remains challenging. This is because multiple DFT calculations, which are necessary in HTCS to determine the thermodynamic and mechanical properties, are computationally expensive and time consuming, limiting the explorable chemical space of MXenes. Therefore, several studies conducting HTCS have focused only on MXenes with specific chemical formulas or have not considered a sufficient variety of transition metals and surface terminations. In particular, Zhan *et al.*[15] conducted HTCS to assess the potential of 72 MXenes as pseudocapacitors using the formula $M_{n+1}X_nT_x$. However, their focus was primarily on iso-stoichiometric MXenes, with limited exploration of other families of non-stoichiometric MXenes, such as those with two different surface terminations. Furthermore, among the large variety of surface terminations, O and OH have been predominantly considered. Similarly, other HTCS studies have explored a limited number of MXenes, focusing on a single family of MXene with the chemical formulas of $M'_2M''C_2T_2$, $M'_2M''_2C_3T_2$,[26] or $M'_2M''CNO_2$.[14] In short, several studies utilizing HTCS have not fully exploited the extensive chemical diversity of MXene families and this limitation has been attributed to the high computational costs of first-principles calculations.

Machine learning (ML) has been extensively used in many studies to overcome the limitations of HTCS and explore a broader chemical space.[27–30] ML offers exceptional inference speed and high prediction accuracy for various material properties, which can complement the computationally expensive DFT calculations that are a bottleneck in the HTCS. By employing ML in the HTCS, DFT calculations are only required for the materials that are predicted by ML as having the highest performance in an application, thus significantly reducing computational time and costs. Therefore, ML enables the fast and efficient screening of materials with a large chemical space. For example, Cai *et al.*[28] used HTCS combined with ML to identify promising cathode candidates for magnesium and zinc batteries from 3880 spinel materials. They successfully identified six spinel materials with remarkable electronic properties and reduced the screening time by approximately 72 years. In the field of 2D materials, Priya *et al.*[29] employed ML to screen 3814 2D materials in terms of the water desalination performance. They discovered several 2D materials, such as FeO_2, CuH_2O_2, and $F_2N_2Ti_3$, that exhibited four times better performance than that of graphene and MoS_2. By incorporating ML into the HTCS, the exploration of materials can be expanded from less than 100 candidates to over 3000, thereby achieving efficient and effective identification of high-performance materials for specific applications.

Inspired by the remarkable usefulness of ML in HTCS, this study proposes a high-throughput MXene screening framework that combines ML and DFT calculations to rapidly evaluate the thermodynamic stability of various MXenes and to explore their mechanical properties. By leveraging the advantages of ML, we could consider 23 857 diverse MXenes as candidates, including

iso-stoichiometric and various non-stoichiometric MXenes as well as MXenes with several types of surface terminations, extending beyond O and OH. Thus, this study could consider significantly more MXenes in terms of their number and diversity when compared to those considered in previous studies. The proposed framework consists of two surrogate ML models that can accurately predict ΔH and ΔH_{hull} of candidate MXenes, which aided in determining the thermodynamic stability of the candidate MXenes. Subsequently, the stability of the MXenes that were deemed to be thermodynamically stable was re-verified using DFT calculations. Then, the mechanical properties such as in-plane stiffness, shear modulus, and Poisson's ratio were determined using DFT calculations. Thus, this framework aims to not only efficiently and rapidly screen MXenes from extensive chemical spaces in terms of their thermodynamic stability, but also evaluate their mechanical robustness.

2. Methods

Fig. 1 shows an overview of this study. The proposed method comprises three steps: data preparation, application of a high-throughput MXene screening framework consisting of ML and DFT screening, and a comprehensive analysis of the thermodynamic, mechanical, and structural properties of MXenes. In this section, the data used in this study, method of feature extraction, ML techniques used for ML screening, and detailed information about the DFT calculations are discussed.

2.1. Database and data processing

In this study, we employed the Computational 2D Materials Database (C2DB)[31] to train two surrogate ML models for predicting ΔH and ΔH_{hull}. Chemical formulas and ΔH and ΔH_{hull} values for 15 733 2D materials were extracted from the C2DB. We then represented each 2D material using 149 features derived from their stoichiometries, employing matminer software[32] for feature generation. These features are designed to capture various characteristics such as chemical compositions of 2D materials, including the types and quantities of the constituent elements, electronegativity difference between them, and number of valence electrons in each orbital. Details of the 149 features used in this work are summarized in ESI† (Sup. 1). These features have been frequently employed when constructing ML models that were used to predict the properties of other crystalline materials such as voltages of electrode materials for metal-ion batteries[33] and ΔH of octahedral 2D materials[34] and those models have shown outstanding prediction performance as well; mean absolute error (MAE) of 0.42 V and 0.099 eV per atom, respectively. Moreover, these features can be readily obtained from just the chemical formula without requiring additional DFT calculations, thereby minimizing the time required to construct the training database. This characteristic makes them especially suitable for a high-throughput screening framework, where fast screening is one of the advantages. Hence, they were used in this study.

Next, we utilized the aNANt database[35] as the target database with the aim to identify thermodynamically stable MXenes and explore their mechanical properties using the framework proposed in this study. The aNANt database contains 23 857 MXenes that represent four families of MXenes: iso-stoichiometric MXenes and three types of non-stoichiometric MXenes, including those with two different surface terminations, two types of transition metals, and distinct surface termination and transition metals (Fig. 2a). Moreover, the MXenes in the aNANt database comprise a wide variety of constituent elements: 11 types each of transition metals and surface terminations (Fig. 2b). Hence, the aNANt database was selected as the target database because it encompasses various MXene families and the chemical space of its constituent

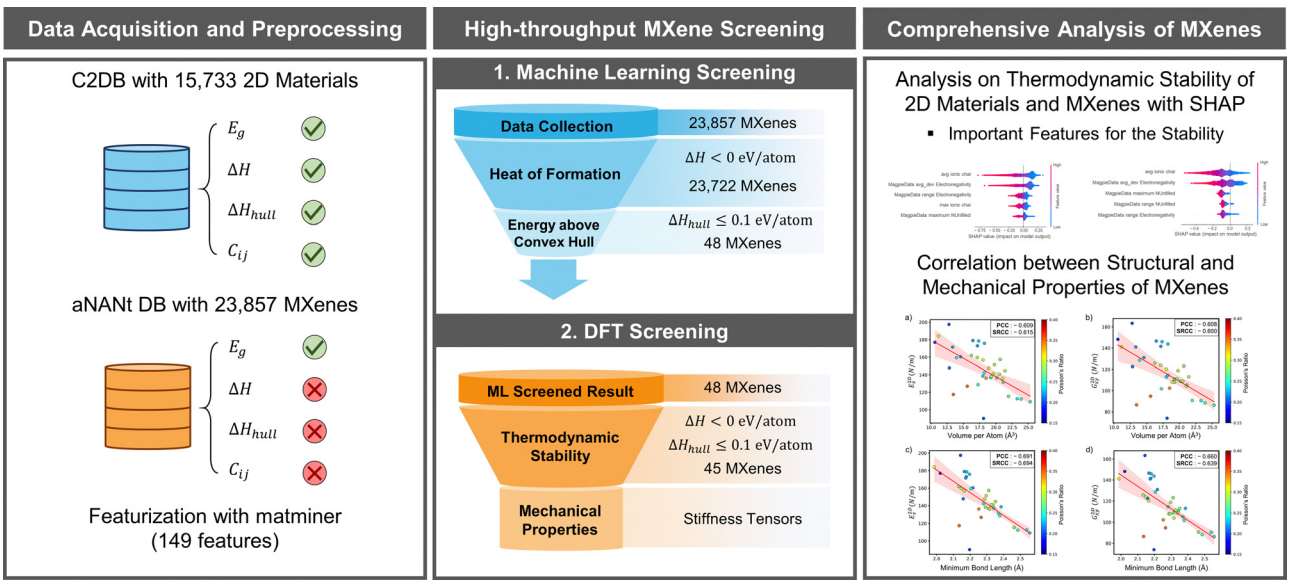

Fig. 1 Overview of this study.

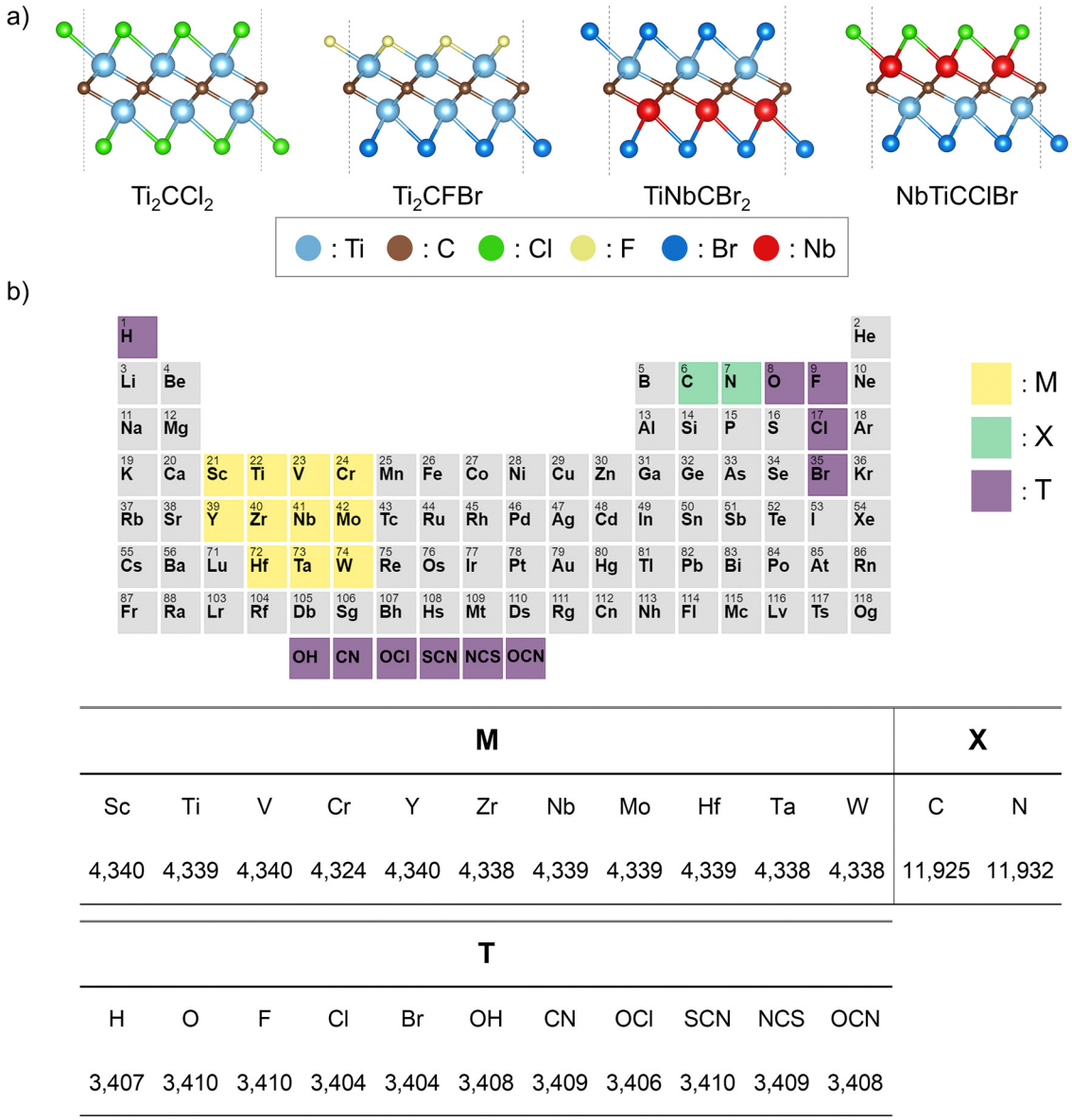

M											X	
Sc	Ti	V	Cr	Y	Zr	Nb	Mo	Hf	Ta	W	C	N
4,340	4,339	4,340	4,324	4,340	4,338	4,339	4,339	4,339	4,338	4,338	11,925	11,932

T										
H	O	F	Cl	Br	OH	CN	OCl	SCN	NCS	OCN
3,407	3,410	3,410	3,404	3,404	3,408	3,409	3,406	3,410	3,409	3,408

Fig. 2 (a) Examples of four representative types of MXenes within the aNANt database: iso-stoichometric MXenes and three non-stoichiometric MXenes. (b) Types of transition metals (M), carbon/nitrogen (X), and surface terminations (T) represented on the periodic table. The table lists the number of MXenes for each type.

elements is considerably broad, allowing it to represent the vast chemical space of MXenes.

Notably, the thermodynamic and mechanical properties of all 23 857 MXenes in the aNANt database have not yet been explored, and the database only provides the bandgaps of these MXenes. We created 149 features for each of the 23 857 MXenes using the same method that was used for the 2D materials in C2DB. The 149 feature types were identical for both datasets and the relationship between these two datasets (*i.e.*, C2DB and aNANt database) is further discussed in ESI† (Sup. 2). By enabling the ML models to learn the relationship between the thermodynamic properties and these 149 features using the C2DB dataset, we could accurately predict the thermodynamic properties of the 23 857 MXenes. Such approach of transferring the knowledge that ML models learned from solving one problem (*i.e.*, predicting thermodynamic properties of 2D materials in C2DB) to a related but different problem (*i.e.*, predicting thermodynamic properties of MXenes in aNANt database) is motivated by the transfer learning technique in ML. Transfer learning is particularly useful when there is abundant information about one problem but scarce information about the other and has been frequently employed in the field of materials science.[29,36–39] Specifically, in the context of 2D materials, Priya *et al.*[29] used similar method to identify 2D materials suitable for water desalination. They trained ML model on a dataset of 257 2D materials from three different classes; namely, graphene derivatives, transition metal dichalcogenides, and nitrides. The trained ML model was then used

to predict the water desalination performance of different classes of 2D materials having different structures or compositions; to be specific, halide complexes, oxide complexes, and lithiates (*i.e.*, $MnLi_2$, $IrLi_2$, and $MoLi_2$). Hence, inspired by these studies, a similar approach was employed.

2.2. Machine learning algorithms

In the proposed high-throughput MXene screening framework, two ML techniques, that is, regression and ensemble voting classification, were used to screen MXenes regarding their ΔH and ΔH_{hull}. First, a regression technique was employed to predict ΔH, and five ML models were constructed for evaluation: random forest (RF), light gradient boosting machine (LGBM), extra trees (ET), decision tree (DT), and *k*-nearest neighbors (KNN) regressors. The performance of each model was assessed using evaluation metrics such as *R*-squared (R^2), MAE, and root mean square error (RMSE). To ensure that the trained ML models could accurately predict ΔH for unseen data points, a five-fold cross-validation procedure was used during the evaluation process. Detailed descriptions on the regression models (*i.e.*, RF, LGBM, ET, DT, and KNN) are presented in ESI† (Sup. 3).

Then, for screening MXenes regarding to determine the ΔH_{hull}, ML ensemble voting classification was used. Initially, we attempted to use regression methods (*i.e.*, RF, LGBM, ET, and CatBoost) to predict ΔH_{hull}; however, the four ML regressors that were designed for ΔH_{hull} predictions did not perform well. (The results obtained when using regression methods to predict ΔH_{hull} are presented in ESI† (Sup. 4).) While ΔH has a direct relationship with constituent elements, making it closely related to the features we used, ΔH_{hull} is correlated to multiple materials that are composed of the same constituent elements but in different combinations. Owing to this complexity, accurate prediction of ΔH_{hull} using only composition-element-based features is challenging. However, the main purpose of building ML models was not to accurately predict the value of ΔH_{hull} itself, but rather to determine the thermodynamic stability based on ΔH_{hull}. Therefore, we designed an ML ensemble voting classification to classify MXenes into two groups: those with $\Delta H_{hull} > 0.1$ eV per atom and those with 0 eV per atom $\leq \Delta H_{hull} \leq 0.1$ eV per atom (the rationale for choosing 0.1 eV per atom as a criterion for thermodynamic stability is described in Section 3.1.2). In ensemble voting classification, the collective knowledge of multiple classifiers is used to make informed decisions. Three ML classifiers (RF, LGBM, and CatBoost) were utilized for this method, where the assigned class for a given data point was determined by consensus, specifically the class agreed upon by at least two of the three classifiers. To validate the performance of each classifier, five-fold cross-validation was implemented, and the accuracy, area under the curve (AUC), recall, and *F*1-score were used as the evaluation metrics.

2.3. Density functional theory calculations

DFT calculations were implemented to perform structural relaxation and obtain the thermodynamic and mechanical properties of MXenes. The Vienna Ab initio Simulation Package (VASP) was used for the DFT calculations by applying the Projector-Augmented-Wave (PAW) method for spin polarization.[40,41] The generalized gradient approximation (GGA) of Perdew–Burke–Ernzerhof (PBE) was selected as the exchange–correlation functional.[42] A plane-wave cutoff of 520 eV was applied during the structural relaxation and thermodynamic property calculations, whereas a larger cutoff of 800 eV was used to determine the mechanical properties of the stable MXenes. The lattice parameters and atomic coordinates were optimized until the total energy difference between self-consistent iterations fell below 10^{-6} eV per cell, and the atomic force tolerance during the relaxation was set to 0.03 eV $Å^{-1}$. The *k*-points of 13 × 13 × 1 were used. Moreover, a substantial vacuum space of 25 Å was implemented in the vertical direction to prevent undesired interactions between repeated layers. The elastic tensor of each MXene sample was obtained by calculating the second derivative of the total energy with respect to the applied strain. Two finite difference steps and atomic movements of 0.02 Å were used for the second-derivative calculations.

ΔH of MXenes was computed by referencing the elemental bulk or molecular structures obtained from the Materials Project,[43] which contains comprehensive information on over 150 000 inorganic materials. The phase diagram for each MXene was also calculated using relevant compounds acquired from the Materials Project and was constructed using the Python Materials Genomics (pymatgen) code[44] to determine the ΔH_{hull} of MXenes.[45,46] Data from the Materials Project was able to be utilized in calculating these two values because the DFT calculation setting used for structural optimization in this study were identical to those used in the Materials Project. The DFT calculation settings were generated through the pymatgen's MPRelaxSet function. This function creates INCAR, KPOINTS, and POTCAR files utilizing parameters used to construct the Materials Project. Moreover, in the process of calculating thermodynamic properties, the MaterialsProjectCompatibility function from pymatgen was employed to ensure compatibility between DFT calculation results of this study and the DFT energies of elements and compounds in the Materials Project. Specifically, the function verified the symbols in the POTCAR files used (*e.g.*, PAW_PBE O 08Apr2002) and checked the run type of the DFT calculation (*e.g.*, GGA). Thus, thanks to these processes, it was possible to utilize information on over 150 000 inorganic materials from the Materials Project for the calculation of thermodynamic properties.

The in-plane stiffness, shear modulus, and Poisson's ratio were computed from the elastic tensors of MXenes. The elastic tensor (C) is a fourth-order tensor and the relationship between the second-order stress (σ) and strain (ε) can be expressed with the elastic tensor as follows:

$$\sigma_{ij} = C_{ijkl}\varepsilon_{kl}$$

Here, i, j, k, l represent Cartesian indices, which can take the values x, y, and z. This equation can be rewritten in Voigt notation under the transformation $xx \rightarrow 1$, $yy \rightarrow 2$, $zz \rightarrow 3$, $yz \rightarrow 4$, $xz \rightarrow 5$, $xy \rightarrow 6$. Because MXenes are 2D materials, components related to the Cartesian index of z can be

disregarded, resulting in the following simplified equation.

$$\begin{bmatrix}\sigma_1\\ \sigma_2\\ \sigma_6\end{bmatrix} = \begin{bmatrix}C_{11} & C_{12} & C_{16}\\ C_{21} & C_{22} & C_{26}\\ C_{61} & C_{62} & C_{66}\end{bmatrix}\begin{bmatrix}\varepsilon_1\\ \varepsilon_2\\ 2\varepsilon_6\end{bmatrix}$$

The in-plane stiffness (E^{2D}), shear modulus (G^{2D}), and Poisson's ratio (ν^{2D}) of MXenes[20] were derived from the above elastic constants using the following equations:

$$E_x^{2D} = \frac{C_{11}C_{22} - C_{12}C_{21}}{C_{22}}, \quad E_y^{2D} = \frac{C_{11}C_{22} - C_{12}C_{21}}{C_{11}},$$

$$G_{xy}^{2D} = C_{66}, \quad \nu_{xy}^{2D} = \frac{C_{21}}{C_{22}}, \quad \nu_{yx}^{2D} = \frac{C_{12}}{C_{22}}$$

3. Results and discussion

3.1. Machine learning screening

3.1.1. Heat of formation. Heat of formation (ΔH) is a crucial thermodynamic property that has been widely used as a criterion to assess the thermodynamic stability of materials.[14,47,48] As ΔH is the energy change associated with the formation of one mole of a compound from its elemental constituents, $\Delta H < 0$ eV per atom implies that the energy is released during the formation, indicating that the resulting compound is more stable than its elemental constituents. Therefore, MXenes with $\Delta H < 0$ eV per atom must be identified within the 23 857 MXenes for further analysis. To achieve this, we first trained the aforementioned five regression models, namely RF, LGBM, ET, DT, and KNN, using 15 733 2D materials in C2DB, enabling the prediction of ΔH based on 149 features for any given 2D material. We validated the performance of these five ML regressors using five-fold cross-validation and the ET regressor demonstrated the best results, with an R^2 of 0.943, MAE of 0.103 eV per atom, and RMSE of 0.164 eV per atom. The validation results for all five regressors and the predictions made by the ET regressor for each data point are shown in Fig. 3. The results evidently demonstrate that the trained ET regressor can accurately predicts ΔH of 2D materials. Details about ET regressor (*e.g.* hyperparameters) are summarized in ESI† (Sup. 5).

Therefore, based on the ET regressor trained on 15 733 2D materials in C2DB, we conducted ΔH predictions for the 23 857 MXenes. Consequently, we confirmed that 23 722 MXenes are thermodynamically stable with $\Delta H < 0$ eV per atom. Conversely, 135 MXenes failed to meet this condition and were excluded from further analysis. This implies that approximately 99.5% of the 23 857 MXenes are likely to undergo an exothermic process upon formation, indicating their stability when compared to that of the constituent elements. Upon closer examination, all the excluded 135 MXenes were found to contain Cr, Mo, or W as a transition metal. Moreover, approximately 90% had a molecular form such as CN, SCN, or NCS, rather than as elements such as O, F, or Br for surface termination. Hence, at this step, it was anticipated that MXenes with these transition metals and surface terminations would be unlikely to achieve thermodynamic stability, which was later proven to be true in Section 3.2. Following this screening step, we recognized the need for additional criteria to assess thermodynamic stability for the following reasons. (1) ΔH is insufficient for completely assessing thermodynamic stability because it only considers the constituting elements and does not account for other competing phases. (2) Although the purpose of screening was to gradually narrow down the candidates to reduce computational cost, it is difficult to say that sufficient screening was carried out solely based on ΔH. Therefore, an additional criterion must be considered to better screen MXenes for thermodynamic stability, which is the energy above the convex hull.

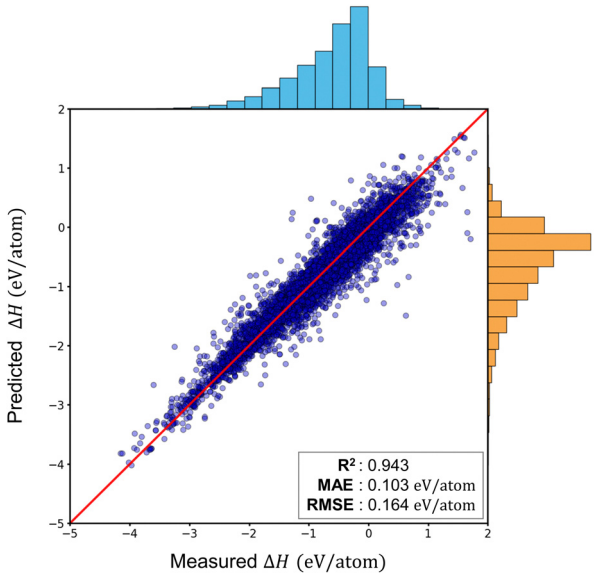

	R^2	MAE (eV/atom)	RMSE (eV/atom)
RF	0.933±0.003	0.117±0.004	0.178±0.006
LGBM	0.939±0.002	0.121±0.002	0.170±0.005
ET	**0.943**±0.003	**0.103**±0.003	**0.164**±0.006
DT	0.866±0.009	0.157±0.004	0.251±0.010
KNN	0.884±0.004	0.165±0.003	0.234±0.002

Fig. 3 Predictions of the trained extra trees (ET) regressor on ΔH of two-dimensional (2D) materials within Computational 2D Materials Database. Histograms at the top and right side represent the distributions of the measured and predicted ΔH values by the ET regressor, respectively. The table presents the performance of the five machine learning regressors that were tested in this study, with the ET regressor showing the best performance.

3.1.2. Energy above the convex hull. The energy above the convex hull (ΔH_{hull}) quantifies the energy difference between competing phases, indicating whether the current configuration is stable or if a more favorable arrangement can be achieved by combining the constituent elements differently. As such, ΔH_{hull} achieves more precise identification of thermodynamically stable materials when compared to ΔH, and has been widely used in various studies.[49–51] $\Delta H_{hull} = 0$ eV per atom indicates that the compound does not decompose into competing phases and is considered stable. 0 eV per atom $< \Delta H_{hull} \leq 0.1$ eV per atom indicates that the compound is

metastable, whereas $\Delta H_{hull} > 0.1$ eV per atom implies instability.[52] In this study, we considered both stable and metastable MXenes because several metastable compounds have been successfully synthesized.[49,52] Therefore, we set the thermodynamic stability criterion as 0 eV per atom $\leq \Delta H_{hull} \leq$ 0.1 eV per atom and this criterion has been widely used in previous studies.[23,24]

To determine whether the ΔH_{hull} values of the 23 722 MXenes with negative heat of formation meet the specified criterion, ensemble voting classification was performed. To train ML classifiers, the datasets from C2DB were first divided into two classes: one with 0 eV per atom $\leq \Delta H_{hull} \leq$ 0.1 eV per atom and the other with $\Delta H_{hull} > 0.1$ eV per atom. Three ML classifiers – RF, LGBM, and CatBoost classifiers – were trained to accurately predict the class in which a 2D material belongs based on the 149 features. We validated the performance of these three ML classifiers using five-fold cross-validation and the results are listed in Table 1. Notably, all three classifiers demonstrated a high level of accuracy of over 80%, and their AUC values were close to 0.9, indicating superior classification performance. Consequently, it was evident that by utilizing the decisions made by these three classifiers, accurate prediction of the range in which ΔH_{hull} of a 2D material belongs is possible. Specific information regarding the three classifiers (*e.g.* hyperparameters) can be found in ESI† (Sup. 5).

Thus, based on the three classifiers trained with 15 733 2D materials in the C2DB, we separated the 23 722 MXenes into two classes according to ΔH_{hull} where they were categorized into the class agreed upon by at least two of the three classifiers using majority voting. Consequently, 48 MXenes were predicted to belong to the class with 0 eV per atom $\leq \Delta H_{hull} \leq 0.1$ eV per atom, and the remaining 23 674 MXenes were excluded from further analysis. Thus, only 0.2% of MXenes were predicted to be stable or metastable based on ΔH_{hull}, and the other MXenes were expected to easily decompose into other competing phases. Thus, we screened a total of 23 857 MXenes based on ΔH and ΔH_{hull} using two ML techniques, and confirmed that only 48 MXenes were more thermodynamically stable than their constituent elements and competing phases. Subsequently, these 48 MXenes were subjected to DFT screening to further validate their thermodynamic stability.

3.2 Density functional theory screening

We performed DFT calculations on the 48 MXenes that were predicted to be thermodynamically stable by the ML models, obtaining their ΔH and ΔH_{hull} for the following reasons. (1) The exact value of ΔH_{hull} was not predicted, so we could not precisely determine whether each MXene is stable or metastable. (2) We planned to upload the thermodynamic and mechanical properties of MXenes obtained in this study to large databases, such as C2DB, thereby contributing to future studies on 2D materials; however, such databases only accept values calculated using DFT. (3) ML models can accurately predict the property values calculated using DFT; however, a degree of error always exists due to discrepancies between training and testing data. Our method of using both ML models and DFT can be viewed as a tradeoff between accuracy and computational cost.

Table 1 Performance of the three classifiers used in ensemble voting classification for classifying two-dimensional materials into two classes

Classifiers	Accuracy	AUC	Recall	*F*1 score
CatBoost	0.844 ± 0.005	0.900 ± 0.008	0.911 ± 0.005	0.891 ± 0.003
LGBM	0.841 ± 0.005	0.901 ± 0.007	0.917 ± 0.005	0.889 ± 0.004
RF	0.833 ± 0.006	0.894 ± 0.011	0.938 ± 0.008	0.887 ± 0.004
Average	0.839	0.898	0.922	0.889

The DFT calculation result showed that all 48 MXenes had $\Delta H < 0$ eV per atom and 45 MXenes had 0 eV per atom $\leq \Delta H_{hull} \leq 0.1$ eV per atom, validating the accuracy of the ML techniques used in this study. The three MXenes that failed to satisfy the ΔH_{hull} criterion were $ScTaCCl_2$, Ti_2NH_2, and Ti_2NO_2. They exhibited ΔH_{hull} values of 0.18, 0.12, and 0.13 eV per atom, respectively, indicating their thermodynamic instability and, therefore, were excluded from further analysis. Among the 45 thermodynamically stable MXenes that were verified to satisfy both criteria based on the DFT calculations, 22 MXenes such as Y_2CCl_2, Hf_2CF_2, and Ti_2NF_2 were previously confirmed to be thermodynamically stable using DFT calculations.[31,53,54] Notably, of these 22 MXenes, 21 were iso-stoichiometric MXenes, implying that previous studies were focused on iso-stoichiometric MXenes. In contrast, the 23 new MXenes that were identified in this study consisted of 18 iso-stoichiometric and 5 non-stoichiometric MXenes with two distinct surface terminations, namely Janus MXenes. Because various non-stoichiometric MXenes were considered in this study, we could identify these five new Janus MXenes to be thermodynamically stable 2D materials. The ΔH and ΔH_{hull} values of the five Janus MXenes and three representative stable iso-stoichiometric MXenes are listed in Table 2. The results of the remaining 15 thermodynamically stable MXenes are described separately in ESI† (Sup. 6). To the best of our knowledge, the thermodynamic and mechanical properties of these 23 MXenes have not yet been calculated using DFT or tested experimentally. This implies that (1) they could contribute to future studies on thermodynamically stable 2D materials and (2) the high-throughput MXene screening framework proposed in this study demonstrated its potential in identifying new thermodynamically stable MXenes.

To further validate the performance of the proposed framework and examine the stability of the 45 thermodynamically stable MXenes, two additional calculations were conducted. Initially, 120 MXenes predicted as unstable through ML screening were randomly selected, and their ΔH_{hull} values were obtained through DFT calculations. Remarkably, all 120 MXenes exhibited ΔH_{hull} values exceeding 0.1 eV per atom, indicating accurate predictions by the proposed framework. Also, the average value was remarkably high at 0.77 eV per atom, reflecting the scarcity of stable MXenes within the considered chemical space; the distribution of the ΔH_{hull} values can be found in ESI† (Sup. 7). Subsequently, phonon information at the Γ-point, obtained while determining the mechanical properties of 45 thermodynamically

Table 2 ΔH and ΔH_{hull} of 8 representative MXenes among 23 MXenes identified to be thermodynamically stable for the first time in this study

MXene	ΔH (eV per atom)	ΔH_{hull} (eV per atom)	MXene type	Thermodynamic stability	Dynamic stability
Hf_2CClBr	−1.46	0.00	Janus	Stable	Stable
Ti_2CClBr	−1.34	0.00	Janus	Stable	Stable
Ti_2NClBr	−1.69	0.00	Janus	Stable	Stable
Ti_2NOH	−1.88	0.10	Janus	Metastable	Stable
Zr_2CClBr	−1.48	0.00	Janus	Stable	Stable
Y_2NBr_2	−1.81	0.00	Iso-stoichiometric	Stable	Stable
Ti_2CBr_2	−1.09	0.00	Iso-stoichiometric	Stable	Stable
Zr_2NCl_2	−2.00	0.00	Iso-stoichiometric	Stable	Stable

stable MXenes, were examined to further assess their stability. All 45 MXenes had positive frequency values at the Γ-point, indicating they are not only thermodynamically but also dynamically stable. The frequency values at the Γ-point for the 23 MXenes identified as stable for the first time in this study are presented in ESI† (Sup.8) and Fig. S3. Furthermore, six out of the 23 MXenes were selected for additional phonon calculations that were based on the finite difference method. Both VASP and PHONOPY[55] were utilized to obtain phonon band structures that can visualize phonon dispersions across high symmetry lines. All six MXenes exhibited positive frequency values across all high symmetry points, reaffirming their dynamic stability, and the frequency values at the Γ-points were consistent with those in Fig. S3 (ESI†). The phonon band structures of the six MXenes are presented in ESI† (Sup.8) and Fig. S4. In conclusion, the results summarized above indicate that the framework successfully identified stable MXenes in the extensive chemical space whose stability was verified thoroughly with both DFT and phonon calculations. Yet, as mentioned earlier, there remains the possibility of finding MXenes that are thermodynamically stable but were predicted as unstable due to the inherent limitations of ML. Therefore, developing ML methods with accuracy and robustness comparable to DFT is also suggested as one direction of future work.

The frequency of each element constituting the 45 stable MXenes is shown in Fig. 4a and the results can be discussed from three perspectives. First, MXenes with transition metals belonging to Groups 3 (Sc, Y) and 4 (Ti, Zr, Hf) comprise the majority of the 45 thermodynamically stable MXenes, with MXenes containing Ti being the most abundant (24%). This result is in strong agreement with those of previous studies. For instance, Li *et al.* had summarized all 37 MXenes that were successfully synthesized in previous research; among them, 12 were MXenes with Ti, which is more than the number of MXenes with other transition metals.[8] This indicates a correlation between the findings of this study and actual synthesis results. Second, most of the 45 thermodynamically stable MXenes had carbon atoms at the X site (64%). Similarly, of the 37 synthesized MXenes, 31 exhibited carbon at the X site.[8] The similarity between the two results demonstrates the effectiveness of the proposed high-throughput MXene screening framework. Finally, the surface terminations of the 45 thermodynamically stable MXenes predominantly comprised Group-17 elements, including F, Cl, and Br (89%). Although only a few experimental research studies on MXenes with F, Cl, and Br as surface terminations have been published, the presence of halogen elements as surface terminations can theoretically maximize the electronegativity difference between the surface termination and the transition metal.[56] Such an increase in the electronegativity difference allows for stronger interactions between them, consequently enhancing the stability of MXenes. The importance of the electronegativity difference in relation to thermodynamic stability is reaffirmed in Section 3.3.1. In summary, the 45 MXenes validated for thermodynamic stability through DFT calculations exhibited a similar trend in chemical composition as that of the experimentally synthesized MXenes. Furthermore, their stability can be theoretically explained. Therefore, we propose the 45 thermodynamically stable MXenes that were identified in this study as highly promising candidates for synthesis.

Conversely, aside from these 45 stable MXenes, the rest which comprise majority within the chemical space explored in this study were predicted as thermodynamically unstable and thus were excluded as the result of ML screening. Such result can also be explained by comparing the chemical space of the MXenes explored in this study and MXenes that have been successfully synthesized. First, from the perspective of constituent elements, according to Anasori *et al.*,[57] who summarized the constituent elements of MXenes that have been successfully synthesized so far, the transition metals considered in this study were mostly those found in successfully synthesized MXenes, except for Sc. However, the synthesized MXenes predominantly had surface terminations of O, OH, F, or Cl while MXenes with other surface terminations are rarely synthesized. Although the chemical space considered in this study did include these four surface terminations, 21 878 MXenes contained at least one surface termination other than these four. In other words, the majority, excluding 1979 MXenes, had surface terminations that are not commonly found in successfully synthesized cases. Second, regarding the types (*i.e.*, stoichiometries) of MXenes considered, it was observed that: (i) Janus MXenes and MXenes with distinct surface terminations and transition metals have not yet been successful synthesized due to the difficulty of composing the bottom and top surfaces of MXenes with different elements or groups.[11,58,59] (ii) For hybrid transition metal MXenes, although there are several cases of successful synthesis,[60–62] most utilized mixed surface terminations, not considering the single element type of surface termination (*i.e.*, uniform surface termination) used in the aNANt database. (iii) Iso-stoichiometric MXenes terminated with a uniform surface termination have been increasingly synthesized recently; synthesized materials

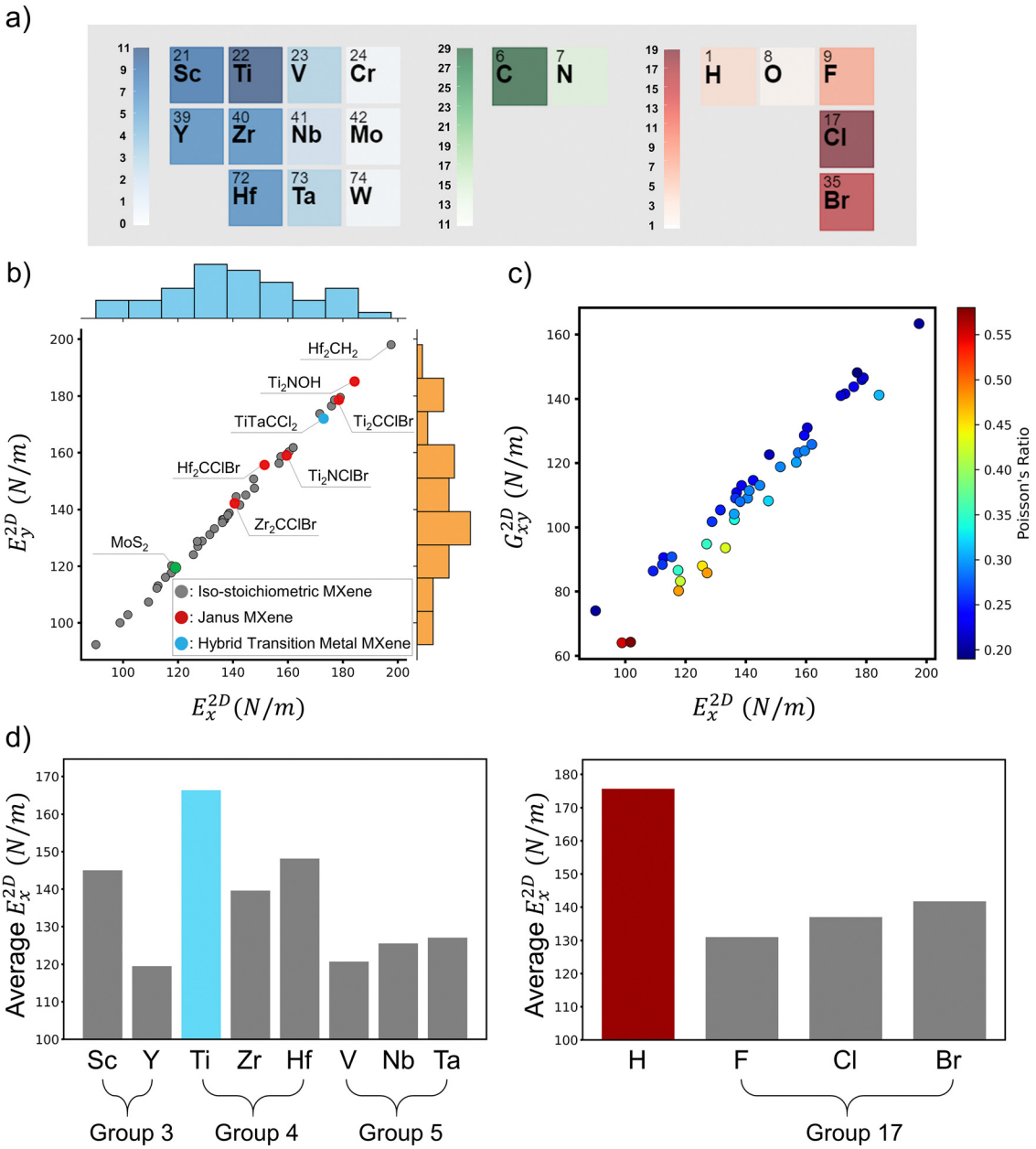

Fig. 4 (a) Number of thermodynamically stable MXenes according to each chemical composition; (b) E_x^{2D} and E_y^{2D} of the 43 thermodynamically stable MXenes; (c) relationship between E_x^{2D} and G_{xy}^{2D}, as well as ν_{xy}^{2D}; (d) average of E_x^{2D} for each chemical composition.

include Nb_2CCl_2, Nb_2CS_2, $Ti_3C_2Cl_2$, Ti_2CCl_2, and $Ti_3C_2I_2$.[8,63–65] Upon comparison, it was found that some, such as Nb_2CCl_2 and Ti_2CCl_2, were successfully identified as thermodynamically stable by the proposed framework and, to the best of our knowledge, none of the MXenes predicted to be unstable have been successfully synthesized. Therefore, the fact that only 45 of the 23 857 MXenes were deemed stable can be attributed to the small subset of these 23 857 MXenes possessing similar constituent elements and stoichiometries to those that were successfully synthesized. The rationale for exploring the chemical space of MXenes in aNANt database despite the differences between them and synthesized MXenes is summarized in ESI† (Sup. 9).

The mechanical properties of the 45 MXenes whose thermodynamic stabilities were validated were calculated using additional DFT calculations. Two MXenes with negative elastic constants were excluded from further consideration; thus, the elastic tensors of the remaining 43 MXenes were obtained. By utilizing these values, the x-direction in-plane stiffness (E_x^{2D}), y-direction in-plane stiffness (E_y^{2D}), shear moduli (G_{xy}^{2D}), and Poisson's ratio (ν_{xy}^{2D}) were obtained, as illustrated in Fig. 4b and c. The E_x^{2D} and E_y^{2D} values of the MXenes were nearly identical, demonstrating their isotropic elastic nature, as previously reported.[20] The in-plane stiffness (E^{2D}) of MXenes ranged from 90.11 to 198.02 N m^{-1}, with Hf_2CH_2 MXene exhibiting the highest E_y^{2D}. Despite their asymmetric structures, the Janus

MXenes (Ti_2NOH, Ti_2CClBr, Ti_2NClBr, Hf_2CClBr, and Zr_2CClBr) and MXenes with two types of transition metals, namely the hybrid transition metal MXene ($TiTaCCl_2$), showed high in-plane stiffness. Specifically, the Janus MXenes exhibited E_x^{2D} values of 184.24, 178.55, 159.54, 151.46, and 140.60 N m^{-1}, respectively, which were higher than the average E_x^{2D} value of 139.03 N m^{-1} of the remaining 37 iso-stoichiometric MXenes. Similarly, $TiTaCCl_2$, a hybrid transition metal MXene, exhibited a high E_x^{2D} of 172.97 N m^{-1}. MoS_2, a widely known 2D material with E^{2D} of 120 N m^{-1}, has been studied for its application in elastic energy storage owing to its high strength and flexibility.[66] Among the 43 stable MXenes, 33 exhibited a higher E^{2D} than MoS_2, suggesting their potential for elastic energy storage, especially when their flexibility, such as ultimate tensile strain, is further investigated in future studies. Moreover, Fig. 4c shows that MXenes with high E^{2D} also tend to exhibit high E_{xy}^{2D}. E_{xy}^{2D} of the stable MXenes ranged from 64.00 to 163.40 N m^{-1}, whereas v_{xy}^{2D}, indicated by the color of the points in Fig. 4c, ranged from 0.19 to 0.58. The wide range of the mechanical properties indicates that the mechanical properties of MXenes can vary extensively based on their chemical composition. E_x^{2D}, E_y^{2D}, E_{xy}^{2D}, and v_{xy}^{2D} for all 43 MXenes are summarized in ESI† (Sup. 10).

After observing the effect of the chemical composition of MXene on its mechanical properties, we calculated the average E^{2D} for each transition metal, X-site atom, and surface termination type. The results are shown in Fig. 4d and they are compared with those of a previous study that theoretically analyzed the mechanical properties of MXenes. Theoretically, E^{2D} of MXenes is closely related to the bonding between the transition metal and the X-site atom and surface termination. The strength of these bonds can be determined based on the bond stiffness, which is derived from the bond energy and bond length. Wyatt *et al.*[9] calculated the bond stiffness between transition metals and carbon or nitrogen in MXenes and determined that titanium exhibited higher bond stiffness with carbon and nitrogen than with other transition metals. They also compared the bond energy between the transition metal and surface termination and observed that the bonds between the transition metals from Group 4 (Ti, Zr, and Hf) and halogen surface terminations (F and Cl) had the highest bond energy. This trend is attributed to the large electronegativity difference between them.[9]

Our study obtained results that align with the aforementioned theoretical analysis. As shown in Fig. 4d, MXenes with transition metals from Group 4 (Ti, Zr, and Hf) exhibit a higher average E_x^{2D} than MXenes with other transition metals. Among them, MXenes with titanium exhibited the highest average E_x^{2D} of 166.34 N m^{-1}, which is consistent with the theoretical analysis presented in a previous study.[9] Notably, among the 43 MXenes calculated for mechanical properties, 38 had halogen surface terminations, which contributed to the higher average E^{2D} of MXenes with transition metals from Group 4, as mentioned by Wyatt *et al.*[9] This suggests that the large electronegativity difference between the surface termination and transition metal plays a role in enhancing E^{2D} of MXenes. Although MXenes with hydrogen surface termination showed a higher average E^{2D} of 175.63 N m^{-1} when compared to that of MXenes with halogen surface terminations (F, Cl, Br), which exhibit average E^{2D} values of 131.04, 137.00, and 141.74 N m^{-1}, respectively, it is important to consider that there were only five MXenes with hydrogen surface terminations in our study. Moreover, research on the mechanical properties of MXenes with hydrogen surface terminations is lacking. Therefore, further investigations such as obtaining uniaxial tensile stress and strain curves using DFT calculations are required to understand their mechanical properties. In summary, the mechanical properties of the 43 MXenes calculated in this study were consistent with the theoretically analyzed results of a previous study, highlighting the significant influence of the chemical composition of an MXene on its mechanical properties. To create MXenes with superior mechanical properties, especially E^{2D}, the following three key approaches can be considered: (1) using transition metals from Group 4, particularly titanium, (2) using halogen elements for surface termination, and (3) considering MXenes with asymmetric structures, such as Janus or hybrid transition metal MXenes. Based on the results of this study, we inferred that by designing the chemical composition of MXenes accordingly, thermodynamically stable and mechanically robust MXenes can be obtained.

3.3. Comprehensive analysis

3.3.1. Thermodynamic stability of two-dimensional materials and MXenes. In the proposed high-throughput MXene screening framework, we utilized the ET regressor that was trained with 2D materials in C2DB to predict ΔH of MXenes. To identify the features that have a significant impact on predicting ΔH and to analyze their relationship with ΔH, we utilized a method known as Shapley Additive Explanations (SHAP).[67] Unlike traditional feature importance methods, such as permutation importance, which focus on single-feature effects, SHAP considers both the main and interaction effects between features, providing a more accurate and consistent attribution of importance. Therefore, this method has been widely applied in multiple materials science studies, revealing various correlations between the material properties.[68,69]

Fig. 5a and b illustrate the most influential features for predictions made by the ET regressor, trained with 2D materials in C2DB, on the training dataset (*i.e.*, 2D materials in C2DB) and the test dataset (*i.e.*, MXenes in the aNANt database), respectively. We highlighted the top-five features in terms of importance, and four of these features are identical in the case of both 2D materials and MXenes. In particular, the electronegativity of constituent elements, total number of unfilled states, and ionic character between the elements were identified as key factors for predicting ΔH. Regarding the electronegativity-related features, the mean absolute deviation and range of electronegativity values of constituent elements exhibited significant feature importance. As the range and mean absolute deviation are both statistical measures that are closely related to the differences among the values, and the ionic character is also associated with the differences in

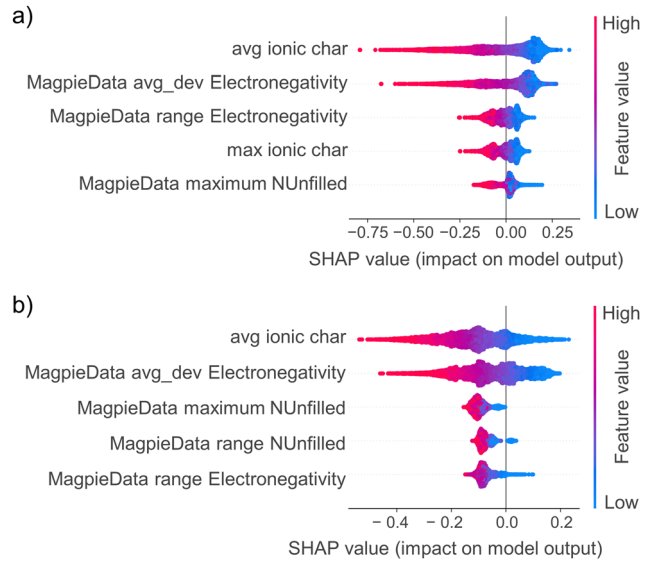

Fig. 5 Five important features for predicting ΔH of (a) 2D materials in C2DB and (b) MXenes in aNANt database that were identified using Shapley Additive Explanations.

electronegativity between constituent elements, it can be inferred that ΔH of 2D materials and MXenes is significantly influenced by the differences in the electronegativity values of their components. A previous study also showed that, in the case of MXenes, if the difference in electronegativity between the transition metal and the surface termination is small, the interaction between the two elements weakens, making it unstable.[56] Hence, larger differences in electronegativity between the constituent elements of MXenes can lead to more stable structures. The SHAP results also illustrate such relationship. Both the mean absolute deviation and range of constituent elements' electronegativities are inversely related to ΔH, meaning that as their values increase, ΔH decreases. As a lower ΔH indicates higher thermodynamic stability, our study reaffirms that 2D materials and MXenes with larger values related to the differences in the electronegativity of constituent elements are more likely to be thermodynamically stable, a useful insight for designing new thermodynamically stable 2D materials.

3.3.2. Mechanical properties of MXenes. We investigated the relationship between the mechanical (specifically, E_x^{2D} and G_{xy}^{2D}) and structural properties of the 43 MXenes. We considered the volume per atom (VPA), minimum bond length, and thickness as the structural properties, which were obtained from MXene structures that were relaxed using DFT calculations. These properties have been widely used to understand the relationship between the structure and mechanical properties of ultrahigh-modulus crystals and inorganic compounds.[70,71] The thickness of an MXene was determined by adding the vertical distance between the topmost and bottommost atoms to the sum of their van der Waals radii. Subsequently, we used this thickness to calculate the VPA by multiplying it with the cross-sectional area of a unit cell. Finally, the minimum bond length is defined as the smallest distance between the atomic nuclei of the atoms composing MXene. Given that ν_{xy}^{2D} of the 43 MXenes ranged broadly from 0.19 to 0.58, we first partitioned the MXenes into two categories based on the mid-range value of 0.38. A total of 36 MXenes fell within this mid-range, whereas 7 MXenes exceeded it.

We then analyzed the correlation between the mechanical properties of the MXenes with ν_{xy}^{2D} less than 0.38 and the aforementioned three structural properties, yielding remarkable results in terms of the Pearson correlation coefficient (PCC) and Spearman rank correlation coefficient (SRCC). As shown in Fig. 6, E_x^{2D} exhibits inverse correlation with VPA (PCC = −0.609, SRCC = −0.615) and minimum bond length (PCC = −0.691, SRCC = −0.694); however, its relationship with MXene thickness (PCC = −0.427, SRCC = −0.474) is not apparent when compared to that of the other two structural properties. Similarly, G_{xy}^{2D} also exhibited a highly negative relationship with VPA (PCC = −0.608, SRCC = −0.600) and minimum bond length (PCC = −0.660, SRCC = −0.639), but not with MXene thickness (PCC = −0.450, SRCC = −0.474). Specifically, VPA demonstrated an inverse relationship with both E_x^{2D} and G_{xy}^{2D}. A smaller VPA indicates that the atoms in the material are tightly bound, resulting in a stronger bond strength. Because a stronger bond strength within molecules yields stronger resistance against deformation, it is theoretically valid that smaller VPA values correspond to better mechanical properties, as supported by previous studies on the mechanical properties of bulk materials and MXenes.[20,70] The minimum bond length also exhibited a similar relationship. Usually, a shorter bond length implies a greater bond stiffness, which in turn indicates a higher resistance to deformation.[72] Hence, smaller bond lengths lead to better mechanical properties; such a relationship has also been shown in a computational study of representative 2D materials.[73]

Conversely, the MXene thickness, whose correlation analysis results are shown in Fig. 6e and f, did not exhibit a clear relationship with the mechanical properties, as it appears to be scattered and exhibits lower PCC and SRCC values than those of the other two structural properties. Through this correlation analysis, we discovered that thermodynamically stable MXenes with ν_{xy}^{2D} less than 0.38, which indicates a relatively lower compressibility, exhibit an inverse association between their mechanical properties and the VPA and minimum bond length. Thus, smaller VPA values and shorter minimum bond lengths are conducive to achieving higher E_x^{2D} and G_{xy}^{2D}. This understanding can be used to quickly identify mechanically robust MXenes in the future by focusing on MXenes with such structural characteristics for mechanical property calculations using DFT.

4. Conclusion

In this work, we developed two surrogate ML models for predicting ΔH and ΔH_{hull}, by leveraging the existing big data on 2D materials, namely C2DB. Using these models with high prediction accuracies (ΔH: R^2 = 0.973, MAE = 0.102 eV per atom; ΔH_{hull}: average accuracy = 0.839, average AUC = 0.898), we could

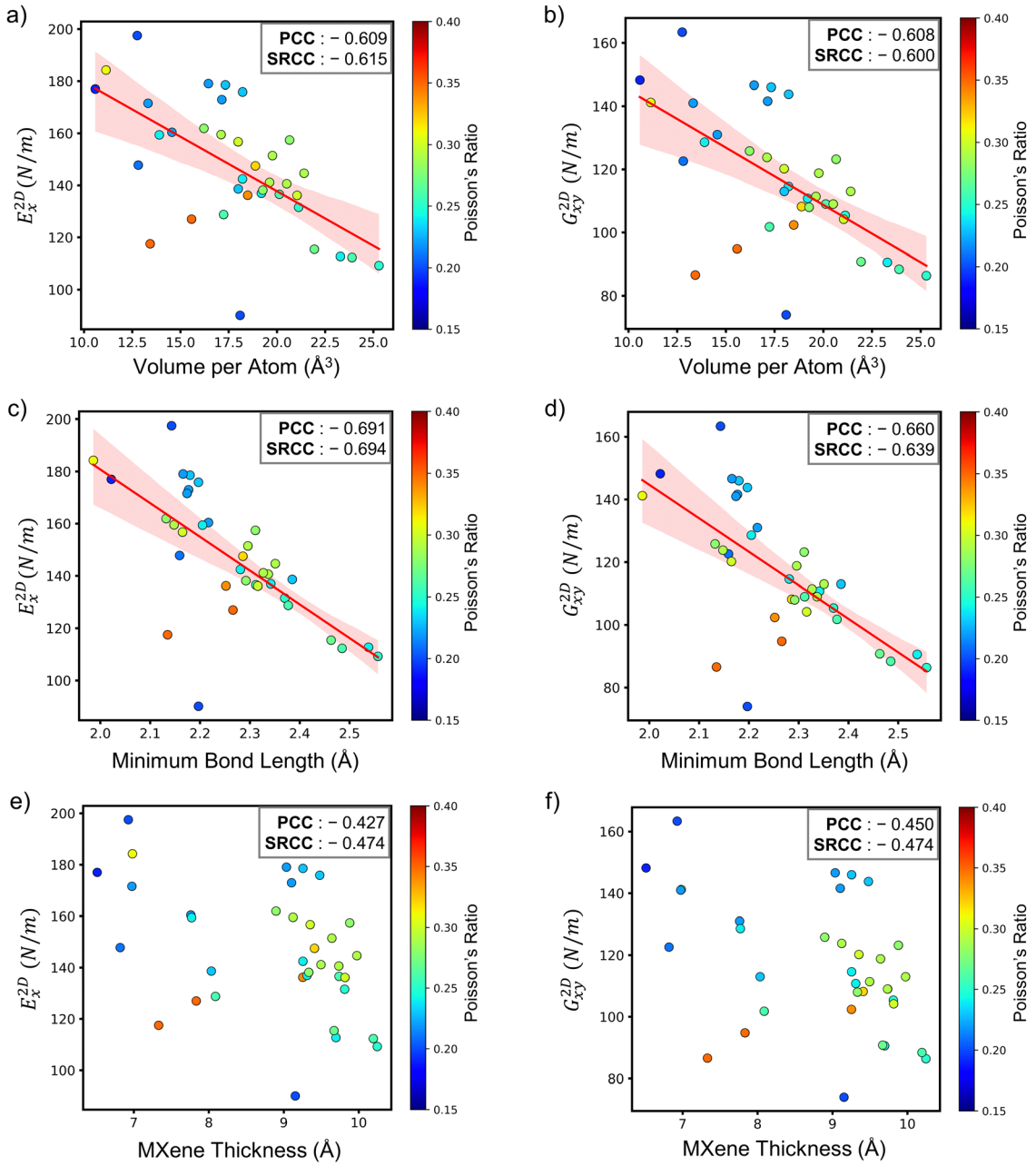

Fig. 6 Correlation between volume per atom and mechanical properties: (a) E_x^{2D} and (b) G_{xy}^{2D}; correlation between minimum bond length and mechanical properties: (c) E_x^{2D} and (d) G_{xy}^{2D}; correlation between MXene thickness and mechanical properties: (e) E_x^{2D} and (f) G_{xy}^{2D}. Red lines are linearly fitted lines, while red areas correspond to the confidence interval band.

expeditiously screen 23 857 MXene to identify 48 MXenes that were predicted to be stable in terms of the ΔH and ΔH_{hull} criteria. Among them, 45 MXenes were verified to be stable using DFT calculations, and their mechanical properties, such as E^{2D}, G_{xy}^{2D}, and ν_{xy}^{2D} were obtained. Based on the above results and a comprehensive analysis of the thermodynamic and mechanical properties of MXenes, the major contributions of this study and corresponding future research directions can be summarized as follows:

• This framework demonstrates significant potential to be used in screening more diverse MXenes, such as high-entropy MXenes, MXenes with more than one layer of carbon or nitrogen ($M_{n+1}X_nT_x$; $n > 1$), and MXenes with late transition metals (Fe, Co, and Ni), which were not investigated in this work. Furthermore, the proposed framework demonstrates notable expandability, allowing it to be adjusted or expanded to suit practical applications. Through simple modifications, it is possible to expeditiously and easily identify MXenes that are thermodynamically stable and simultaneously possess properties suitable for practical applications, with detailed methods for these modifications presented in ESI† (Sup. 11).

• The 23 MXenes that were identified as stable for the first time in this study exhibited a similar chemical composition

trend to the experimentally synthesized MXenes, and their stability could be theoretically explained. Also, MXenes with halogen surface terminations have recently been studied as cathodes for Zinc ion batteries (ZIB).[74] Therefore, we propose that these MXenes are highly promising candidates for synthesis and their potential as cathodes for ZIB should be explored by obtaining their electrochemical properties through DFT calculations.

• Through both compositional analysis and SHAP, the importance of the electronegativity difference between the constituent elements of MXene on the thermodynamic stability was highlighted. Maximizing the electronegativity difference between the transition metals and surface terminations is the key to designing stable MXenes.

• The following three approaches for designing MXenes with high E^{2D} and G_{xy}^{2D} were identified:

(1) Using transition metals from Group 4, especially Ti.

(2) Using surface terminations that have high bond energies with selected transition metals (halogen surface terminations for Group-4 transition metals).

(3) Minimizing VPA and minimum bond length of MXenes.

Data availability

The thermodynamic and mechanical properties data of the MXenes explored in this study are all available in ESI.†

Conflicts of interest

There are no conflicts to declare.

Acknowledgements

This work was supported in part by the National Research Foundation of Korea (NRF) grant funded by the Korea government (Ministry of Science and ICT) (No. 2022R1C1C1009387, No. 2022R1F1A1074339), in part by the Institute of Civil Military Technology Cooperation funded by the Defense Acquisition Program Administration and Ministry of Trade, Industry, and Energy (MOTIE) of the Korea government under grant No. 19-CM-GU-01 and in part by the Korea Institute of Energy Technology Evaluation and Planning (KETEP) grant funded by the Korea government (MOTIE) under grant No. 20206610100290.

References

1 M. Naguib, M. Kurtoglu, V. Presser, J. Lu, J. Niu, M. Heon, L. Hultman, Y. Gogotsi and M. W. Barsoum, Two-dimensional nanocrystals produced by exfoliation of Ti_3AlC_2, *Adv. Mater.*, 2011, **23**(37), 4248–4253.

2 D. Er, J. Li, M. Naguib, Y. Gogotsi and V. B. Shenoy, Ti_3C_2 MXene as a high capacity electrode material for metal (Li, Na, K, Ca) ion batteries, *ACS Appl. Mater. Interfaces*, 2014, **6**(14), 11173–11179.

3 S. Lee, S. C. Jung and Y.-K. Han, Fe_2 CS_2 MXene: a promising electrode for Al-ion batteries, *Nanoscale*, 2020, **12**(9), 5324–5331.

4 J. Zheng, X. Sun, C. Qiu, Y. Yan, Z. Yao, S. Deng, X. Zhong, G. Zhuang, Z. Wei and J. Wang, High-throughput screening of hydrogen evolution reaction catalysts in MXene materials. The, *J. Phys. Chem. C*, 2020, **124**(25), 13695–13705.

5 M. Khazaei, M. Arai, T. Sasaki, M. Estili and Y. Sakka, Two-dimensional molybdenum carbides: potential thermoelectric materials of the MXene family, *Phys. Chem. Chem. Phys.*, 2014, **16**(17), 7841–7849.

6 D. Huang, H. Kim, G. Zou, X. Xu, Y. Zhu, K. Ahmad, Z. A. Almutairi and H. N. Alshareef, All-MXene thermoelectric nanogenerator, *Mater. Today Energy*, 2022, **29**, 101129.

7 Y. Gogotsi and Q. Huang, *MXenes: two-dimensional building blocks for future materials and devices*, ACS Publications, 2021, vol. 15, pp. 5775–5780.

8 X. Li, Z. Huang, C. E. Shuck, G. Liang, Y. Gogotsi and C. Zhi, MXene chemistry, electrochemistry and energy storage applications, *Nat. Rev. Chem.*, 2022, **6**(6), 389–404.

9 B. C. Wyatt, A. Rosenkranz and B. Anasori, 2D MXenes: tunable mechanical and tribological properties, *Adv. Mater.*, 2021, **33**(17), 2007973.

10 S. Özcan and B. Biel, Exploring a novel class of Janus MXenes by first principles calculations: structural, electronic and magnetic properties of Sc_2 CXT, X = O, F, OH; T = C, S, N, *Phys. Chem. Chem. Phys.*, 2023, **25**, 1881–1888.

11 W. Jin, S. Wu and Z. Wang, Structural, electronic and mechanical properties of two-dimensional Janus transition metal carbides and nitrides, *Phys. E*, 2018, **103**, 307–313.

12 B. Anasori, Y. Xie, M. Beidaghi, J. Lu, B. C. Hosler, L. Hultman, P. R. Kent, Y. Gogotsi and M. W. Barsoum, Two-dimensional, ordered, double transition metals carbides (MXenes), *ACS Nano*, 2015, **9**(10), 9507–9516.

13 X. Zhao, P. Wang, E. Lv, C. Wu, K. Ma, Z. Gao, I. D. Gates and W. Yang, Screening MXenes for novel anode material of lithium-ion batteries with high capacity and stability: A DFT calculation, *Appl. Surf. Sci.*, 2021, **569**, 151050.

14 Z. Zeng, X. Chen, K. Weng, Y. Wu, P. Zhang, J. Jiang and N. Li, Computational screening study of double transition metal carbonitrides M′ 2M″ CNO2-MXene as catalysts for hydrogen evolution reaction, *npj Comput. Mater.*, 2021, **7**(1), 80.

15 C. Zhan, W. Sun, P. R. Kent, M. Naguib, Y. Gogotsi and D.-e Jiang, Computational screening of MXene electrodes for pseudocapacitive energy storage, *J. Phys. Chem. C*, 2018, **123**(1), 315–321.

16 M. Pandey and K. S. Thygesen, Two-dimensional MXenes as catalysts for electrochemical hydrogen evolution: A computational screening study, *J. Phys. Chem. C*, 2017, **121**(25), 13593–13598.

17 X.-Y. Yang, W. Luo and R. Ahuja, Fluoride ion batteries: Designing flexible M_2CH_2 (M= Ti or V) MXenes as high-capacity cathode materials, *Nano Energy*, 2020, **74**, 104911.

18 Y. Li, L. Li, R. Huang, Y. Zhang and Y. Wen, Computational screening of pristine and functionalized ordered TiVC

MXenes as highly efficient anode materials for lithium-ion batteries, *Nanoscale*, 2021, **13**(5), 2995–3001.
19 S. Guha, A. Kabiraj and S. Mahapatra, High-throughput design of functional-engineered MXene transistors with low-resistive contacts, *npj Comput. Mater.*, 2022, **8**(1), 202.
20 S. Tian, K. Zhou, C.-Q. Huang, C. Qian, Z. Gao and Y. Liu, Investigation and understanding of the mechanical properties of MXene by high-throughput computations and interpretable machine learning, *Extreme Mech. Lett.*, 2022, **57**, 101921.
21 Z. Jing, X. Feng, Y. Qiu, N. Li, K. Wu, Y. Cheng and B. Xiao, Screening of 225 Double-Transition-Metal o-MXenes for Superior Thermoelectric Property at Room Temperature from First-Principles Electron and Phonon Calculations, *J. Phys. Chem. C*, 2023, **127**(29), 14125–14136.
22 L. Zhang, C. Tang, C. Zhang and A. Du, First-principles screening of novel ferroelectric MXene phases with a large piezoelectric response and unusual auxeticity, *Nanoscale*, 2020, **12**(41), 21291–21298.
23 J. Kim, E. Kim and K. Min, Synthesizable Double Perovskite Oxide Search via Machine Learning and High-Throughput Computational Screening, *Adv. Theory Simul.*, 2021, **4**(10), 2100263.
24 Y. Song, J. Pan, Y.-F. Zhang, H. Yang and S. Du, Monolayer iridium sulfide halides with high mobility transport anisotropy and highly efficient light harvesting, *J. Phys. Chem. Lett.*, 2021, **12**(25), 6007–6013.
25 N. Sun, Q. Zhu, B. Anasori, P. Zhang, H. Liu, Y. Gogotsi and B. Xu, MXene-bonded flexible hard carbon film as anode for stable Na/K-ion storage, *Adv. Funct. Mater.*, 2019, **29**(51), 1906282.
26 D. Jin, L. R. Johnson, A. S. Raman, X. Ming, Y. Gao, F. Du, Y. Wei, G. Chen, A. Vojvodic and Y. Gogotsi, Computational screening of 2D ordered double transition-metal carbides (MXenes) as electrocatalysts for hydrogen evolution reaction. The, *J. Phys. Chem. C*, 2020, **124**(19), 10584–10592.
27 G. R. Schleder, C. M. Acosta and A. Fazzio, Exploring two-dimensional materials thermodynamic stability via machine learning, *ACS Appl. Mater. Interfaces*, 2019, **12**(18), 20149–20157.
28 J. Cai, Z. Wang, S. Wu, Y. Han and J. Li, A Machine Learning Shortcut for Screening the Spinel Structures of Mg/Zn Ion Battery Cathodes with a High Conductivity and Rapid Ion Kinetics, *Energy Storage Mater.*, 2021, **42**, 277–285.
29 P. Priya, T. C. Nguyen, A. Saxena and N. R. Aluru, Machine learning assisted screening of two-dimensional materials for water desalination, *ACS Nano*, 2022, **16**(2), 1929–1939.
30 C. M. Acosta, E. Ogoshi, J. A. Souza and G. M. Dalpian, Machine learning study of the magnetic ordering in 2D materials, *ACS Appl. Mater. Interfaces*, 2022, **14**(7), 9418–9432.
31 M. N. Gjerding, A. Taghizadeh, A. Rasmussen, S. Ali, F. Bertoldo, T. Deilmann, N. R. Knøsgaard, M. Kruse, A. H. Larsen and S. Manti, Recent progress of the computational 2D materials database (C2DB), *2D Mater.*, 2021, **8**(4), 044002.
32 L. Ward, A. Dunn, A. Faghaninia, N. E. Zimmermann, S. Bajaj, Q. Wang, J. Montoya, J. Chen, K. Bystrom and M. Dylla, Matminer: An open source toolkit for materials data mining, *Comput. Mater. Sci.*, 2018, **152**, 60–69.
33 R. P. Joshi, J. Eickholt, L. Li, M. Fornari, V. Barone and J. E. Peralta, Machine learning the voltage of electrode materials in metal-ion batteries, *ACS Appl. Mater. Interfaces*, 2019, **11**(20), 18494–18503.
34 R. Kumar and A. K. Singh, Chemical hardness-driven interpretable machine learning approach for rapid search of photocatalysts, *npj Comput. Mater.*, 2021, **7**(1), 197.
35 A. C. Rajan, A. Mishra, S. Satsangi, R. Vaish, H. Mizuseki, K.-R. Lee and A. K. Singh, Machine-learning-assisted accurate band gap predictions of functionalized MXene, *Chem. Mater.*, 2018, **30**(12), 4031–4038.
36 R. Ma, Y. J. Colon and T. Luo, Transfer learning study of gas adsorption in metal–organic frameworks, *ACS Appl. Mater. Interfaces*, 2020, **12**(30), 34041–34048.
37 V. V. Korolev, A. Mitrofanov, E. I. Marchenko, N. N. Eremin, V. Tkachenko and S. N. Kalmykov, Transferable and extensible machine learning-derived atomic charges for modeling hybrid nanoporous materials, *Chem. Mater.*, 2020, **32**(18), 7822–7831.
38 A. E. Sifain, N. Lubbers, B. T. Nebgen, J. S. Smith, A. Y. Lokhov, O. Isayev, A. E. Roitberg, K. Barros and S. Tretiak, Discovering a transferable charge assignment model using machine learning, *J. Phys. Chem. Lett.*, 2018, **9**(16), 4495–4501.
39 I. A. Moses, R. P. Joshi, B. Ozdemir, N. Kumar, J. Eickholt and V. Barone, Machine learning screening of metal-ion battery electrode materials, *ACS Appl. Mater. Interfaces*, 2021, **13**(45), 53355–53362.
40 G. Kresse and J. Furthmüller, Efficiency of ab-initio total energy calculations for metals and semiconductors using a plane-wave basis set, *Comput. Mater. Sci.*, 1996, **6**(1), 15–50.
41 G. Kresse and J. Furthmüller, Efficient iterative schemes for ab initio total-energy calculations using a plane-wave basis set, *Phys. Rev. B: Condens. Matter Mater. Phys.*, 1996, **54**(16), 11169.
42 J. P. Perdew, K. Burke and M. Ernzerhof, Generalized gradient approximation made simple, *Phys. Rev. Lett.*, 1996, **77**(18), 3865.
43 A. Jain, S. P. Ong, G. Hautier, W. Chen, W. D. Richards, S. Dacek, S. Cholia, D. Gunter, D. Skinner and G. Ceder, Commentary: The Materials Project: A materials genome approach to accelerating materials innovation, *APL Mater.*, 2013, **1**(1), 011002.
44 S. P. Ong, W. D. Richards, A. Jain, G. Hautier, M. Kocher, S. Cholia, D. Gunter, V. L. Chevrier, K. A. Persson and G. Ceder, Python Materials Genomics (pymatgen): A robust, open-source python library for materials analysis, *Comput. Mater. Sci.*, 2013, **68**, 314–319.
45 S. P. Ong, L. Wang, B. Kang and G. Ceder, Li– Fe– P– O_2 phase diagram from first principles calculations, *Chem. Mater.*, 2008, **20**(5), 1798–1807.
46 A. Jain, G. Hautier, S. P. Ong, C. J. Moore, C. C. Fischer, K. A. Persson and G. Ceder, Formation enthalpies by mixing GGA and GGA+ U calculations, *Phys. Rev. B: Condens. Matter Mater. Phys.*, 2011, **84**(4), 045115.

47 W. Ma, M. Wang, Q. Yi, D. Huang, J. Dang, Z. Lv, X. Lv and S. Zhang, A new Ti2V0. 9Cr0. 1C2Tx MXene with ultrahigh gravimetric capacitance, *Nano Energy*, 2022, **96**, 107129.
48 M.-Z. Liu, X.-H. Li, X.-H. Cui, H.-T. Yan, R.-Z. Zhang and H.-L. Cui, The influence of different functional groups on quantum capacitance, electronic and optical properties of Hf2C MXene, *Appl. Surf. Sci.*, 2022, **605**, 154830.
49 H. Park, C. J. Bartel, G. Ceder and P. Zapol, Layered Transition Metal Oxides as Ca Intercalation Cathodes: A Systematic First-Principles Evaluation, *Adv. Energy Mater.*, 2021, **11**(48), 2101698.
50 S. Li, Z. Chen, W. Zhang, S. Li and F. Pan, High-throughput screening of protective layers to stabilize the electrolyte-anode interface in solid-state Li-metal batteries, *Nano Energy*, 2022, **102**, 107640.
51 R. Jacobs, T. Mayeshiba, J. Booske and D. Morgan, Material discovery and design principles for stable, high activity perovskite cathodes for solid oxide fuel cells, *Adv. Energy Mater.*, 2018, **8**(11), 1702708.
52 W. Sun, S. T. Dacek, S. P. Ong, G. Hautier, A. Jain, W. D. Richards, A. C. Gamst, K. A. Persson and G. Ceder, The thermodynamic scale of inorganic crystalline metastability, *Sci. Adv.*, 2016, **2**(11), e1600225.
53 S. Haastrup, M. Strange, M. Pandey, T. Deilmann, P. S. Schmidt, N. F. Hinsche, M. N. Gjerding, D. Torelli, P. M. Larsen and A. C. Riis-Jensen, The Computational 2D Materials Database: high-throughput modeling and discovery of atomically thin crystals, *2D Mater.*, 2018, **5**(4), 042002.
54 P. Lyngby and K. S. Thygesen, Data-driven discovery of 2D materials by deep generative models, *npj Comput. Mater.*, 2022, **8**(1), 232.
55 A. Togo, L. Chaput, T. Tadano and I. Tanaka, Implementation strategies in phonopy and phono3py, *J. Phys.: Condens. Matter*, 2023, **35**, 353001.
56 L. Wang, S. Gao, W. Li, A. Zhu, H. Li, C. Zhao, H. Zhang, W.-H. Wang and W. Wang, Machine learning assisted screening of MXenes pseudocapacitive materials, *J. Power Sources*, 2023, **564**, 232834.
57 B. Anasori and Û. G. Gogotsi, *2D metal carbides and nitrides (MXenes)*, Springer, 2019, vol. 416.
58 B. Akgenç, E. Vatansever and F. Ersan, Tuning of electronic structure, magnetic phase, and transition temperature in two-dimensional Cr-based Janus MXenes, *Phys. Rev. Mater.*, 2021, **5**(8), 083403.
59 M. Das and S. Ghosh, Improved charge storage capacity of supercapacitor electrodes by engineering surfaces: the case of Janus MXenes, *J. Phys. Chem. C*, 2024, **128**(3), 1014–1023.
60 Q. He, H. Hu, J. Han and Z. Zhao, Double transition-metal TiVCTX MXene with dual-functional antibacterial capability, *Mater. Lett.*, 2022, **308**, 131100.
61 L. Wang, M. Han, C. E. Shuck, X. Wang and Y. Gogotsi, Adjustable electrochemical properties of solid-solution MXenes, *Nano Energy*, 2021, **88**, 106308.
62 W. Hong, B. C. Wyatt, S. K. Nemani and B. Anasori, Double transition-metal MXenes: Atomistic design of two-dimensional carbides and nitrides, *MRS Bull.*, 2020, **45**(10), 850–861.
63 M. Li, X. Li, G. Qin, K. Luo, J. Lu, Y. Li, G. Liang, Z. Huang, J. Zhou and L. Hultman, Halogenated Ti3C2 MXenes with electrochemically active terminals for high-performance zinc ion batteries, *ACS Nano*, 2021, **15**(1), 1077–1085.
64 V. Kamysbayev, A. S. Filatov, H. Hu, X. Rui, F. Lagunas, D. Wang, R. F. Klie and D. V. Talapin, Covalent surface modifications and superconductivity of two-dimensional metal carbide MXenes, *Science*, 2020, **369**(6506), 979–983.
65 Y. Li, H. Shao, Z. Lin, J. Lu, L. Liu, B. Duployer, P. O. Persson, P. Eklund, L. Hultman and M. Li, A general Lewis acidic etching route for preparing MXenes with enhanced electrochemical performance in non-aqueous electrolyte, *Nat. Mater.*, 2020, **19**(8), 894–899.
66 Q. Peng and S. De, Outstanding mechanical properties of monolayer MoS 2 and its application in elastic energy storage, *Phys. Chem. Chem. Phys.*, 2013, **15**(44), 19427–19437.
67 S. M. Lundberg and S.-I. Lee, A unified approach to interpreting model predictions, in *Advances in neural information processing systems*, 2017, p. 30.
68 H. Tang, Q. Xu, M. Wang and J. Jiang, Rapid screening of metal–organic frameworks for propane/propylene separation by synergizing molecular simulation and machine learning, *ACS Appl. Mater. Interfaces*, 2021, **13**(45), 53454–53467.
69 C. Zhi, S. Wang, S. Sun, C. Li, Z. Li, Z. Wan, H. Wang, Z. Li and Z. Liu, Machine-Learning-Assisted Screening of Interface Passivation Materials for Perovskite Solar Cells, *ACS Energy Lett.*, 2023, **8**(3), 1424–1433.
70 Q. Shao, R. Li, Z. Yue, Y. Wang and E. Gao, Data-driven discovery and understanding of ultrahigh-modulus crystals, *Chem. Mater.*, 2021, **33**(4), 1276–1284.
71 M. De Jong, W. Chen, T. Angsten, A. Jain, R. Notestine, A. Gamst, M. Sluiter, C. Krishna Ande, S. Van Der Zwaag and J. J. Plata, Charting the complete elastic properties of inorganic crystalline compounds, *Sci. Data*, 2015, **2**(1), 1–13.
72 M. Kaupp, B. Metz and H. Stoll, Breakdown of Bond Length-Bond Strength Correlation: A Case Study, *Angew. Chem., Int. Ed.*, 2000, **39**(24), 4607–4609.
73 P. Hess, Bonding, structure, and mechanical stability of 2D materials: the predictive power of the periodic table, *Nanoscale Horiz.*, 2021, **6**(11), 856–892.
74 Y. Guo, Z. Du, Z. Cao, B. Li and S. Yang, MXene Derivatives for Energy Storage and Conversions, *Small Methods*, 2023, 2201559.